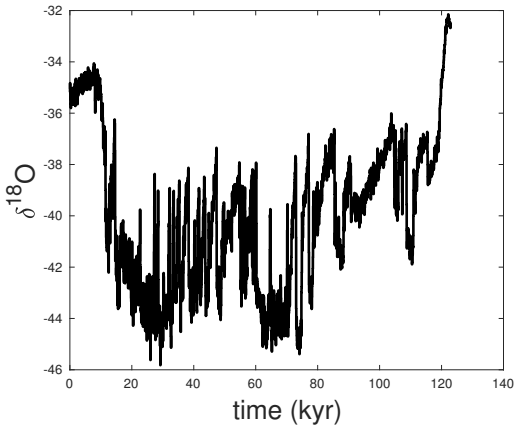

FIGURE 10. *Oxygen isotope anomaly ($\delta^{18}O$) from the NGRIP ice core (Andersen & et al. 2004). Peak to peak temperature changes between 50 ky and 20 ky are about 10° C.*

4. Dansgaard-Oeschger Events

4.1. *Phenomena*

Isotope analyses from ice cores on Greenland provide information on the local temperatures over the last 100 ky. The local oxygen isotope anomalies ($\delta^{18}O$) from the NGRIP ice core are plotted in Fig. 10. Slow variations are associated with the development of the last ice age of which the extremum occurred around 25 ky. The relatively rapid transitions (for example between 50 ky and 20 ky) with an equivalent peak-to-peak amplitude of about 10°C are called the Dansgaard-Oeschger events (Oeschger *et al.* 1984). There has been an extensive discussion on the dominant time scale of these events (Wunsch 2000). Through careful analysis of the GISP2 (Stuiver & Grootes 2000) record, Schultz (2002) concludes that between 46 and 13 ky, the onset of Dansgaard-Oeschger events was paced by a fundamental period of ∼1470 years. Before 50 ky, the presence of such a dominant period is unclear due to dating uncertainties in the ice core record.

The behavior of the climate system on millennial time scales during the last glacial period is highly interesting for an understanding of feedbacks between the ocean, atmosphere and cryosphere. There are many indications from proxy data that there have been large-scale reorganizations of both the atmosphere and ocean associated with Dansgaard-Oeschger events and a review is provided in Clement & Peterson (2008). In the subpolar North Atlantic, Dansgaard-Oeschger events were matched with corresponding sea surface temperature changes of at least 5°C. A theory of Dansgaard-Oeschger events will have to explain at least the processes controlling the dominant ∼1500 year time scale of the variability and the asymmetric character of the transition with a rapid warming and a relatively slow cooling phase. As discussed in Clement & Peterson (2008), several different views have been proposed to explain the millennial climate variability during the last glacial period. Leading theories all involve changes in the Atlantic Ocean circulation.

4.2. *The Atlantic Meridional Overturning Circulation*

On the large scale, the ocean circulation is driven by momentum fluxes (by the wind), the tides and affected by fluxes of heat and freshwater at the ocean-atmosphere interface. The buoyancy fluxes affect the surface density of the ocean water and through mixing and advection, density differences are propagated horizontally and vertically. In the North Atlantic, the Gulf Stream transports relatively warm and saline waters northwards. Part of the heat is taken up by the atmosphere, making the water denser. In certain

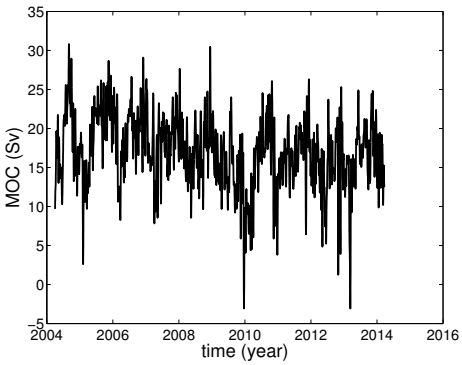

FIGURE 11. *Volume transport of the Atlantic MOC at 26°N as measured by the RAPID-MOCHA array from April 2004 to April 2014 (Smeed* et al. *2014).*

areas (e.g. the Labrador Sea), when there is strong cooling in winter, the water column becomes unstably stratified resulting in strong convection (Marshall & Schott 1999). The interaction of this convection with boundary currents (Spall 2003) eventually leads to the formation of deepwater, which overflows the various ridges that are present in the topography and enters the Atlantic basin.

This deepwater is transported southwards at a depth of about 2 km, where it enters the Southern Ocean. Through upwelling in the Atlantic, Pacific and Indian Ocean, the water is slowly brought back to the surface (Talley 2008). To close the mass balance the water eventually is transported back in the upper ocean to the sinking areas in the North Atlantic. In the Southern Ocean, also bottom water is formed which has a higher density than that from the northern North Atlantic and therefore appears in the abyssal Atlantic and Pacific. In the North Pacific no deep water is formed.

The Atlantic Meridional Overturning Circulation (MOC) is the zonally integrated volume transport, characteristic by the meridional overturning stream function. This transport is mainly responsible for the meridional heat transport in the Atlantic. The strength and spatial pattern of the MOC are determined by density differences which set up pressure differences in the Atlantic. There are no observations available to reconstruct the pattern of the MOC but its strength at 26°N in the Atlantic is now routinely monitored by the RAPID-MOCHA array (Cunningham *et al.* 2007; Srokosz & Bryden 2015). The currently available time series of the MOC strength is shown in Fig. 11 indicating a mean of about 19 Sv, a standard deviation of 5 Sv and a decreasing trend of about 1.6 Sv over the last decade (Smeed *et al.* 2014). At 26°N the heat transport associated with the Atlantic MOC is estimated to be 1.2 PW (Johns *et al.* 2011). This heat is transferred to higher latitudes leading to a relatively mild climate over Western Europe, compared to similar latitudes on the eastern Pacific coast.

4.3. *Stochastic Conceptual Models*

The simplest picture one can imagine that captures the key aspects of the MOC can be traced back to Stommel (1961). It is reasonable to suppose that the transport between equatorial and polar water reservoirs depends upon their mutual density difference $\Delta\rho$. A physical reason for this is that denser polar water is more pre-conditioned to convect to the ocean floor, enhancing meridional overturning. Stommel supposed the existence of two reservoirs of water, one representing the poles and the other the equator, with temperatures and salinities T_p, S_p and T_e, S_e, respectively (see Fig. 12).

The density of seawater is approximated following a simple linear dependence upon T and S,

$$\rho = \rho_0 - \alpha_T(T - T_0) + \alpha_s(S - S_0), \tag{4.1}$$

where the thermal expansivity α_T and salinity coefficients α_s are assumed constant. One may then express the density difference between the two reservoirs as

$$\Delta\rho = -\alpha_T(T_p - T_e) + \alpha_s(S_p - S_e), \tag{4.2}$$

which in turn governs the transport rate per unit volume $Q(\Delta\rho)$.

The two reservoirs do not only interact with each other, but are individually forced at their upper surface. The temperature is supposed to relax, over a timescale t_r, to the local atmospheric temperature T_a, which is formulated as $T_a = T_0 - \theta/2$ for the polar box and $T_a = T_0 + \theta/2$ for the equatorial box. Whereas colder water will have greater tendency to draw in heat than warmer water, salty water does not stimulate the atmosphere to rain on it! Consequently, salinity forcing is poorly modelled as a relaxation to some equilibrium value. A more physical form for the forcing is chosen whereby a prescribed flux $F_S/2$ of fresh water enters the polar ocean (in the form of rain, meltwater, etc.), with an equal volume (for simplicity) leaving at the equator by evaporation ($-F_S/2$). As S_0 is the typical value of salinity in the ocean, the result of the freshwater flux is a decrease in salinity in the polar box with rate proportional to $F_S S_0$ and an equivalent increase in the equatorial box.

The equations governing the two-box system are then (Cessi 1994)

$$\dot{T}_e = -\frac{1}{t_r}[T_e - (T_0 + \tfrac{1}{2}\theta)] - \frac{Q(\Delta\rho)}{2}(T_e - T_p), \tag{4.3a}$$

$$\dot{S}_e = +\frac{F_S}{2H}S_0 - \frac{Q(\Delta\rho)}{2}(S_e - S_p) \tag{4.3b}$$

$$\dot{T}_p = -\frac{1}{t_r}[T_p - (T_0 - \tfrac{1}{2}\theta)] - \frac{Q(\Delta\rho)}{2}(T_p - T_e), \tag{4.3c}$$

$$\dot{S}_p = -\frac{F_S}{2H}S_0 - \frac{Q(\Delta\rho)}{2}(S_p - S_e) \tag{4.3d}$$

where H is the ocean depth. We can now see that in the form written above, $Q(\Delta\rho)$ must be positive. The reason for this is that although Q is physically the advection of water between two reservoirs, this advection is closed, with as much going in as is coming out for each reservoir. If you reverse the direction of circulation the quantity of polar water moving into the equator and vice versa remain unchanged. With this in mind, considering the simplicity of the model, we are free to choose a functional form for Q that depends only on the magnitude of $\Delta\rho$. In Cessi (1994), the form

$$Q(\Delta\rho) = \frac{1}{t_d} + \frac{q}{\rho_0^2 V}(\Delta\rho)^2, \tag{4.4}$$

is chosen where V is the volume of each reservoir, q is a dimensional transport coefficient and t_d is the timescale of diffusive mixing between the two reservoirs that would occur in the absence of a density difference.

It is convenient to define the temperature and salinity differences

$$\Delta T \equiv T_e - T_p, \qquad \Delta S \equiv S_e - S_p \tag{4.5}$$

and work in terms of these variables. From equations 4.3, we obtain the time evolution

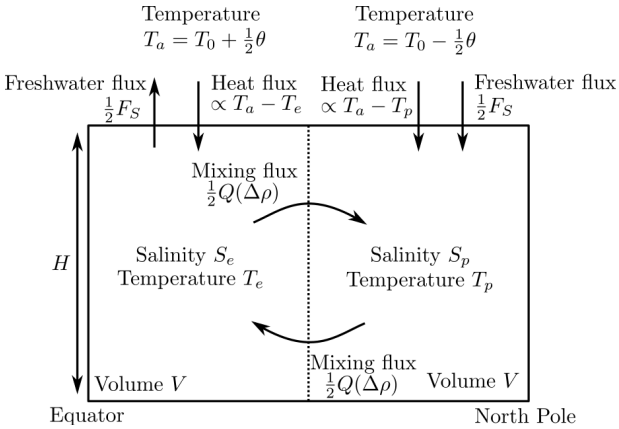

FIGURE 12. Schematic of the Stommel two-box model of the meridional overturning circulation

of the temperature and salinity differences:

$$\frac{d\Delta T}{dt} = -\frac{1}{t_r}(\Delta T - \theta) - Q(\Delta\rho)\Delta T, \tag{4.6a}$$

$$\frac{d\Delta S}{dt} = \frac{F_s}{H}S_0 - Q(\Delta\rho)\Delta S. \tag{4.6b}$$

Next appropriate scales are introduced to reduce the dynamical variables ΔT and ΔS, together with time t, to their respective dimensionless forms. Appropriate choices are as follows

$$x \equiv \frac{\Delta T}{\theta}, \qquad y \equiv \frac{\alpha_s \Delta S}{\alpha_T \theta}, \qquad t' \equiv \frac{t}{t_d}. \tag{4.7}$$

Once scaled, the dynamical equations for $x(t')$ and $y(t')$ read

$$\dot{x} = -\alpha(x-1) - x\big[1 + \mu^2(x-y)^2\big], \tag{4.8a}$$

$$\dot{y} = F - y\big[1 + \mu^2(x-y)^2\big], \tag{4.8b}$$

where

$$\alpha = \frac{t_d}{t_r}, \qquad \mu^2 = \frac{q t_d (\alpha_t \theta)^2}{V}, \qquad F = \frac{\alpha_s S_0 t_d}{\alpha_t \theta H} F_S. \tag{4.9}$$

The parameter α is the ratio of the diffusive timescale to the timescale over which temperature would exponentially decay to the local atmospheric value. The parameter μ measures the strength of the buoyancy-driven convection between the two basins relative to the diffusive mixing. The parameter F measures the strength of freshwater forcing. Standard values of the two-box model parameters can be found in Table 2.

We may simplify the equation above by noting that for parameters typical of the real ocean (see table) $\alpha \gg 1$, which means that the reservoirs will equilibrate with their local forcing temperatures much more rapidly than they are likely to mix each other's temperatures. Therefore, we may suppose that x remains close to 1 which reduces the problem to an ODE in $y(t)$ alone (where we drop the primes on t' for convenience):

$$\frac{dy}{dt} = F - y\left[1 + \mu^2(1-y)^2\right]. \tag{4.10}$$

If we suppose for now that $F = \bar{F}$ is independent of time, we can represent the time

Parameter	Meaning	Value	Unit
t_r	temperature relaxation timescale	25	days
H	mean ocean depth	4,500	m
t_d	diffusion time scale	180	years
t_a	advection time scale	29	years
q	transport coefficient	1.92×10^{12}	$\mathrm{m^3 s^{-1}}$
V	ocean volume	$300 \times 4.5 \times 8,250$	$\mathrm{km^3}$
α_T	thermal expansion coefficient	10^{-4}	$\mathrm{K^{-1}}$
α_S	haline contraction coefficient	7.6×10^{-4}	–
S_0	reference salinity	35	$\mathrm{g\,kg^{-1}}$
θ	meridional temperature difference	25	K

TABLE 2. Parameters of the Stommel two-box model.

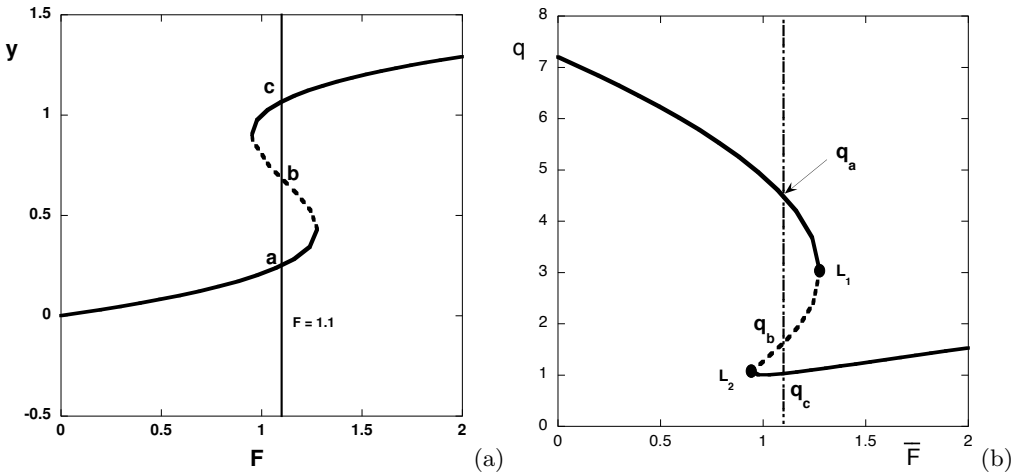

FIGURE 13. *Bifurcation diagram of the model (4.10) for* $\mu^2 = 6.2$*, showing (a)* y *and (b)* $q = 1 + \mu(1-y)^2$ *versus* $\bar{F}$*.*

evolution of y using a potential function $V(y)$:

$$\frac{dy}{dt} = -V'(y), \qquad \text{where } V(y) = -\bar{F}y + \frac{1}{2}y^2 + \mu^2\left(\frac{1}{4}y^4 - \frac{2}{3}y^3 + \frac{1}{2}y^2\right), \tag{4.11}$$

and its derivative with respect to y is denoted by the prime. The potential $V(y)$ is a so-called double-well potential with two stable minima and an unstable maximum. In order to transition from one potential well to the other, a finite amplitude "kick" in y is required.

Recalling that y is simply the dimensionless salinity difference, we immediately see that the two reservoirs can remain in a stable state with either a large salinity difference or a small one. Physically, these correspond to the following: The poles are colder and fresher than the equator. and if we freshen the poles, we increase ΔS, but because temperature drives the convection, this freshening reduces $\Delta\rho$ and so the MOC weakens. Therefore, the higher (lower) value of y is usually referred to as the off (on) state of circulation. Another way to look at it is that in order to balance the freshwater forcing at a large ΔS we need less mixing between the reservoirs than if we have a smaller ΔS. Ultimately, the conclusion here is that the meridional overturning circulation can jump between the on

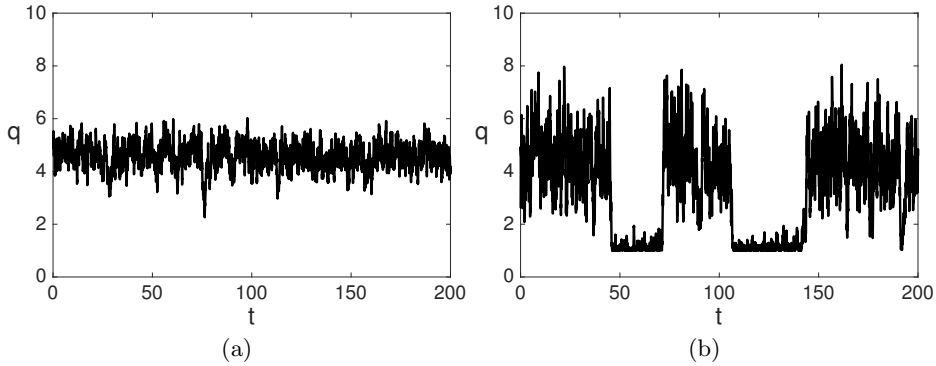

FIGURE 14. *(a) Realization of the box model starting at* $y_a = 0.24$ *for* $\bar{F} = 1.1$, $\mu^2 = 6.2$ *and (a)* $\sigma = 0.1$ *and (b)* $\sigma = 0.25$.

and off states impulsively, given a finite-amplitude perturbation, such as a particularly large ice-melt event.

As an alternative to the potential $V(y)$, one can also plot the steady solutions $\bar{y}$ of the equation (4.10) i.e. solutions of

$$\bar{F} - y(1 + \mu^2(1-y)^2) = 0, \tag{4.12}$$

versus $\bar{F}$. This bifurcation diagram, where both y (Fig. 13a) and the dimensionless volume transport $q = 1 + \mu(1-y)^2$ (Fig. 13b) is used, indeed shows that there is an interval of values $\bar{F}$ for which there are multiple equilibria. Here the dashed states are unstable and the drawn states are stable. The interval of multiple states is bounded by two so-called saddle-node bifurcation points L_1 and L_2.

4.4. *Transitions*

Of course, the freshwater forcing F is unlikely to have been constant in reality and next, we consider F to vary stochastically. This component is represented as white noise with amplitude σ such that $F = \bar{F} + \sigma\xi(t)$. This leads to the Itô equation

$$dY_t = -V'(Y_t)\,dt + \sigma\,dW_t. \tag{4.13}$$

Note here that the result of adding fluctuations to F is additive noise in the equation for Y, rather than noise in the potential $V(y)$.

Starting at one fixed point $y_a = 0.24$, two transient solutions of (4.13) for $\bar{F} = 1.1$, $\mu^2 = 6.2$ are plotted in Fig. 14, one for $\sigma = 0.1$ and one for $\sigma = 0.25$. The transient solution for $\eta = 0.1$ does not make any transition and stays near the equilibrium $y_a = 1.07$ ($q_a = 4.58$). As can be seen, the trajectory for $\sigma = 0.25$ undergoes transitions between the two stable states (y_c and y_a). Clearly the transitions in Fig. 14b are noise induced transitions as the value of $\bar{F}$ is still in the multiple equilibrium regime and smaller than the $\bar{F}$ value at the saddle node bifurcation L_1 (Fig. 13).

As we have seen in section 3, we can write down the forward Fokker-Planck equation in order to solve for the probability density function $p(y,t)$ of the process Y_t, i.e.,

$$\frac{\partial p}{\partial t} = \frac{\partial}{\partial y}\Big(V'(y)p\Big) + \frac{1}{2}\sigma^2\frac{\partial^2 p}{\partial y^2}. \tag{4.14}$$

Now, in the deterministic case before, we sought time-independent solutions for y. Of course, it makes no sense to look for truly time-independent solutions for the random variable Y_t, but a *statistically steady* solution may be found by setting $\partial p/\partial t = 0$ and

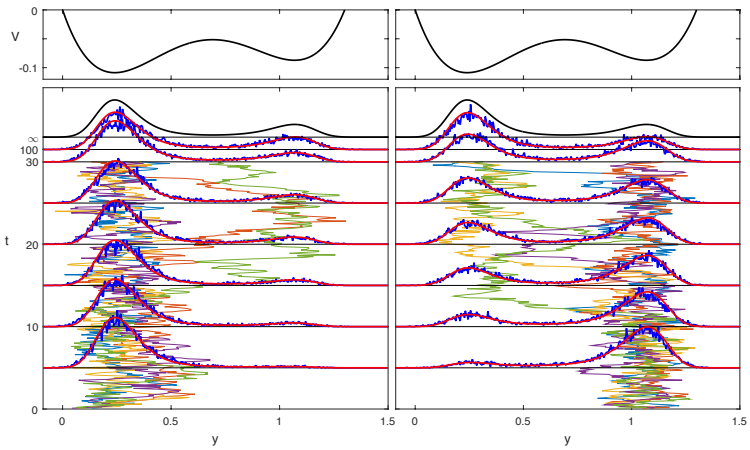

FIGURE 15. *Motion in the double-well potential $V(y)$ from (4.11) with $\bar{F} = 1.1$ and $\mu^2 = 6.2$. Top: Potential $V(y)$. Bottom: Stochastic motion (4.13) with noise amplitude $\sigma = 0.2$ starting from $Y_0 = 0$ (left) or $Y_0 = 1$ (right). The time evolution of five realizations are shown, as well as histograms (blue) from $10,000$ realizations and the probability density (red) obtained from numerical solution of the corresponding Fokker–Planck equation (4.14). The distribution labelled $t = \infty$ is the steady-state distribution $p_s(y)$ from (4.15).*

solving for the function $p_s(y)$ satisfying stationary statistics. The solution method is similar to that for the Ornstein-Uhlenbeck process and the result is,

$$p_s(y) = Ce^{-\frac{2}{\sigma^2}V(y)}, \text{ where } C = \left(\int_{-\infty}^{\infty} e^{-\frac{2}{\sigma^2}V(y)}\, dy\right)^{-1} \tag{4.15}$$

is the normalization coefficient and we have used the boundary condition that $p \to 0$ as $y \to \pm\infty$.

Numerical results for equations (4.13) and (4.14) are shown in Fig. 15. The histograms and probability densities are initially peaked at the well near which the system was launched, indicating that the peak at $y = y_b$ is difficult to cross. They do eventually spread out, though, and attain the steady state given by equation 4.15. In this state, the system typically fluctuates around in one of the two wells and randomly transitions between them, while spending more time overall in the deeper well.

4.5. *Escape time*

Suppose we are in the "on"-state $y = y_a$ of the meridional overturning but subject the system to given, stochastic freshwater forcing. How long is it likely to take for the system to flip into the other ("off") state $y = y_c$? To solve this exit-time problem, let the time when the particle leaves the interval (also referred to as the first exit time) be indicated by $T(y)$. It can be shown that the mean time $\bar{T}(y)$ required to escape to y_c when starting from y satisfies the equation:

$$-1 = -V'\bar{T}' + \tfrac{1}{2}\sigma^2\bar{T}'', \qquad \text{with} \qquad \bar{T}(y_c) = 0, \qquad \bar{T}'(-\infty) = 0, \tag{4.16}$$

where the boundary conditions state that it takes no time to reach y_c when starting from y_c, and that the escape time varies very little for y far below the potential well at y_a since the restoring deterministic drift is very strong there.

The equation is a linear first-order equation for $\bar{T}'(y)$ which we solve by multiplying

by the integrating factor $\exp(-2V(y)/\sigma^2)$:

$$-e^{-\frac{2}{\sigma^2}V} = e^{-\frac{2}{\sigma^2}V}\left(-V'\bar{T}' + \frac{\sigma^2}{2}\bar{T}''\right) = \frac{\sigma^2}{2}\left(e^{-\frac{2}{\sigma^2}V}\bar{T}'\right)'. \tag{4.17}$$

Integration of both sides and using the boundary condition $\bar{T}'(-\infty) = 0$ yields

$$\bar{T}'(y) = e^{\frac{2}{\sigma^2}V(y)}\int_{-\infty}^{y} -\frac{2}{\sigma^2}e^{-\frac{2}{\sigma^2}V(s)}\,ds = -\frac{2}{\sigma^2}\int_{-\infty}^{y} e^{\frac{2}{\sigma^2}[V(y)-V(s)]}\,ds. \tag{4.18a}$$

A second integration using $\bar{T}(y_c) = 0$ yields

$$\bar{T}(y) = -\frac{2}{\sigma^2}\int_{z=y_c}^{y}\int_{s=-\infty}^{z} e^{\frac{2}{\sigma^2}[V(z)-V(s)]}\,ds\,dz. \tag{4.19}$$

Hence the mean escape time from the "on" state $y = y_a$ to the "off" state $y = y_c$ is

$$\bar{T}(y_a) = \frac{2}{\sigma^2}\int_{z=y_a}^{y_c}\int_{s=-\infty}^{z} \exp\left(\frac{2}{\sigma^2}[V(z) - V(s)]\right)\,ds\,dz. \tag{4.20}$$

An asymptotic approximation to the above integral can be obtained in the limit of small noise, where σ^2 is much smaller than the typical variation $V(y_b) - V(y_a)$ of the potential, so that we can treat $M = 2/\sigma^2$ as a large parameter. In this case, the main contribution to the integral in equation 4.20 comes from the region where the exponent $M[V(z) - V(s)]$ is maximal, i.e. $z \approx y_b$ and $s \approx y_a$. The contributions from any other regions are exponentially small and can be ignored. We can thus approximate the result as

$$\bar{T}(y_a) \approx M\int_{y_b-\epsilon}^{y_b+\epsilon} e^{MV(z)}\,dz\int_{y_a-\epsilon}^{y_a+\epsilon} e^{-MV(s)}\,ds, \tag{4.21}$$

where $\epsilon > 0$ is small.

After a change of variables $z = y_b + x$ or $s = y_a + x$, the two integral factors in equation (4.21) have the form

$$I \equiv \int_{-\epsilon}^{\epsilon} e^{Mf(x)}\,dx, \tag{4.22}$$

where $M \gg 1$ and $f(x) = V(y_b + x)$ or $f(x) = -V(y_a + x)$ has a maximum at $x = 0$. We have argued that almost all of the contribution to the integral I comes from the region near this maximum, so we may Taylor expand $f(x)$ as $f(x) \approx f(0) + f''(0)x^2/2$, where no linear term is present and $f''(0) < 0$ since $x = 0$ is a maximum. After the expansion, we can extend the limits to infinity, again because the contributions from regions away from the exponential maximum near $x = 0$ are negligible, and hence

$$\int_{-\epsilon}^{\epsilon} e^{Mf(x)}\,dx \approx e^{Mf(0)}\int_{-\epsilon}^{\epsilon} e^{-\frac{1}{2}M|f''(0)|x^2}\,dx \tag{4.23a}$$

$$\approx e^{Mf(0)}\int_{-\infty}^{\infty} e^{-\frac{1}{2}M|f''(0)|x^2}\,dx \tag{4.23b}$$

$$\approx e^{Mf(0)}\sqrt{\frac{2\pi}{M|f''(0)|}}, \tag{4.23c}$$

where we have made use of the standard result $\int_{-\infty}^{\infty} e^{-\alpha x^2}\,dx = \sqrt{\pi/\alpha}$.

The two integral factors in equation 4.21 are thus

$$\int_{y_b-\epsilon}^{y_b+\epsilon} e^{MV(z)}\,dz \approx \sqrt{\frac{2\pi}{M|V''(y_b)|}}e^{MV(y_b)}, \tag{4.24a}$$

$$\int_{y_a-\epsilon}^{y_a+\epsilon} e^{-MV(s)}\,ds \approx \sqrt{\frac{2\pi}{M|V''(y_a)|}}e^{-MV(y_a)}, \tag{4.24b}$$

and hence the mean escape time from the "on" state $y = y_a$ to the "off" state $y = y_c$ is approximately

$$\bar{T}(y_a) = 2\pi\sqrt{\frac{1}{|V''(y_a)|\,|V''(y_b)|}}\exp\left(\frac{2}{\sigma^2}\left[V(y_b) - V(y_a)\right]\right). \tag{4.25}$$

From the calculations, we can see that this escape time is the same from any state in the well near $y = y_a$ over the peak $y = y_b$ to any state in the well near $y = y_c$. This is in line with our intuition that, for weak noise, the deterministic drift quickly drives the system to the bottom of the well $y = y_a$ where it fluctuates until eventually a large enough random perturbation kicks the system over the crest $y = y_b$ and it falls into the other well $y = y_c$.

4.6. *Periodic forcing and noise*

Within the autonomous framework above, the system will jump between on and off states stochastically, but will not display any dominant time scale (e.g. periodic behaviour), as is observed for Dansgaard-Oeschger events. We therefore augment the previous model with a periodic modulation to the deterministic part of the freshwater forcing, so that

$$F = \bar{F} + \sigma\xi(t) + A\sin\left(2\pi\frac{t}{T}\right), \tag{4.26}$$

where A is the amplitude of periodic forcing and T is the dimensionless period of forcing (as we are still working with dimensionless variables). The governing equation is thus $dy/dt = -dV/dy + \sigma\xi(t)$, where the potential $V(y,t)$ is chosen as

$$V(y,t) = -\bar{F}y + \frac{1}{2}y^2 + \mu^2\left(\frac{1}{4}y^4 - \frac{2}{3}y^3 + \frac{1}{2}y^2\right) - A\sin\left(2\pi\frac{t}{T}\right)(y - 0.7). \tag{4.27}$$

In Fig. 16, we show what happens for a small periodic forcing ($A = 0.05$) to the mean forcing $\bar{F}$ for various values of the noise amplitude σ. For small noise, the system remains in the deeper well most of the time as expected. For large noise, the probability density system frequently transitions between the two wells, almost as if the middle peak at $y = y_b$ did not exist, and the periodicity is quite weak. However, for an intermediate value of noise strength, we recover periodic behaviour on the timescale T. The response is not a small perturbation, but a jump between on and off states every cycle. We have ended up with a system exhibiting so-called 'stochastic resonance', whereby the noise is just large enough to switch between states almost every time the background forcing oscillates.

To explain this mechanism in more details, consider the slightly simplified system with potential

$$V(y) = -\frac{y^2}{2} + \frac{y^4}{4} - \epsilon y\cos(\Omega\tau)$$

Note that the fixed points location (defined by $V'(y) = 0$ and $V''(y) > 0$) do not

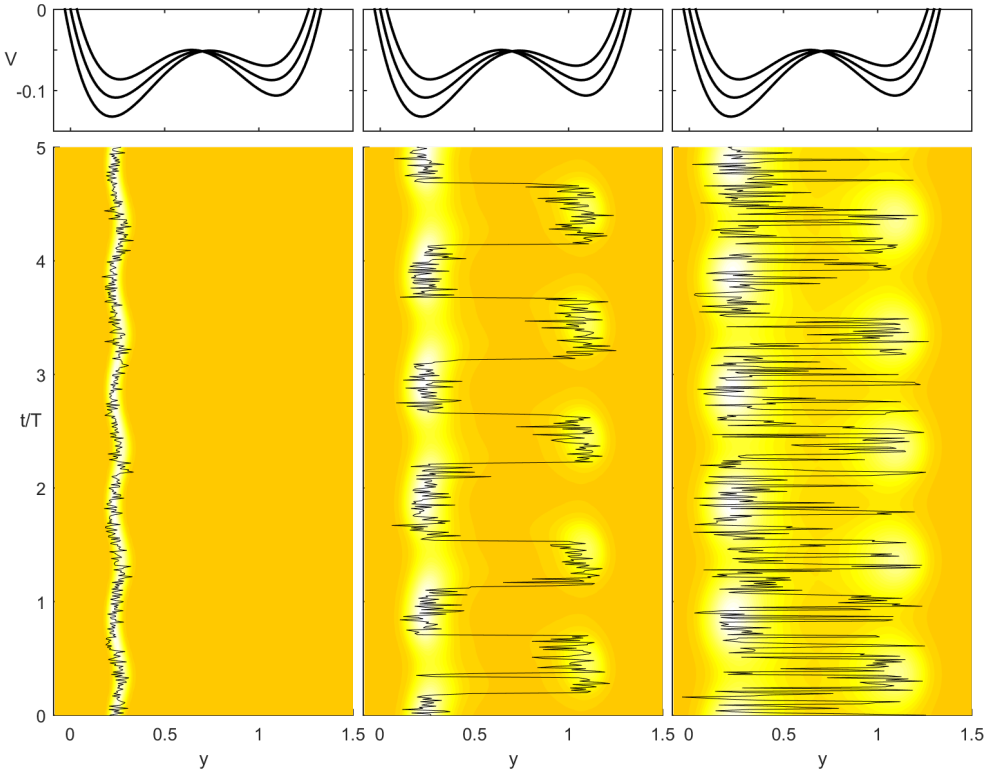

FIGURE 16. *Motion in a time-periodic double-well potential (equation 4.27 with* $\bar{F} = 1.1$, $\mu^2 = 6.2$ *and* $A = 0.05$*). Top: The potential* V *at* $t = -T/2,\ 0,\ T/2$*. Bottom: Stochastic motion with noise amplitude* $\sigma = 0.05$ *(left),* $\sigma = 0.15$ *(middle),* $\sigma = 0.25$ *(right). The time evolution of one realization is shown (black curve), as well as the probability density (heat map) obtained from evolving the corresponding Fokker–Planck equation forward until a time-periodic state is reached. The period* T *chosen corresponds to* 100 000 *years.*

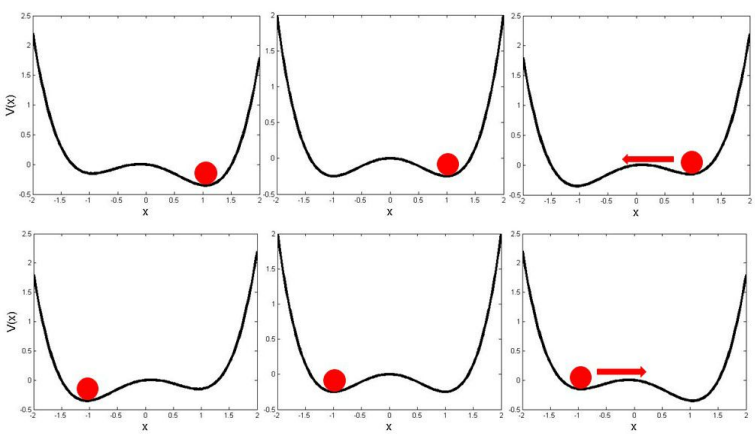

FIGURE 17. Upper: $V(y)$ vs y for $\tau = 0$ (left) $\tau = \frac{\pi}{2\Omega}$ (middle) and $\tau = \frac{\pi}{\Omega}$ (right). Lower: $V(y)$ vs y for $\tau = \frac{\pi}{\Omega}$ (left) $\tau = \frac{3\pi}{2\Omega}$ (middle) and $\tau = \frac{2\pi}{\Omega}$ (right). The state of the system is represented by the red dot.

strongly vary with τ if the amplitude ϵ is small (in which case the fixed points are given by $y_\pm \approx \pm 1$), unlike the value of the potential V at this fixed points. For $\epsilon \ll 1$, these two values are approximately given by:

$$V(y_\pm) \approx V(\pm 1) = -[\frac{1}{4} \pm \epsilon \cos(\Omega\tau)]$$

Using the Laplace approximation, the transition times are approximately given by:

$$< t_{-1\to 1} > \approx 2\pi \sqrt{\frac{1}{-V''(0)V''(-1)}} \exp\{\frac{2[V(0) - V(-1)]}{\sigma^2}\} \approx \sqrt{2}\pi \exp[\frac{1 - 4\epsilon\cos(\Omega\tau)}{2\sigma^2}]$$

$$< t_{1\to -1} > \approx 2\pi \sqrt{\frac{1}{-V''(0)V''(1)}} \exp\{\frac{2[V(0) - V(1)]}{\sigma^2}\} \approx \sqrt{2}\pi \exp[\frac{1 + 4\epsilon\cos(\Omega\tau)}{2\sigma^2}]$$

The transition times vary with τ as the potential changes shape. Because the variance in the transition time is very small compared to the transition time itself, the transition occurs over a small time-interval. As a consequence, the Fourier spectrum has a strong peak at the forcing frequency Ω. In the case of a small periodic forcing ϵ, the synchronization can occur for moderate values of σ.

For example, if we take the small amplitude to be $\epsilon = 0.1$, the shape of the potential is very close to a double well. If we suppose that at $\tau = 0$, the state of the system is near $y_+ \approx 1$, the transition time $< t_{1\to -1} >$ at this τ is maximal, as the potential well is deepest. If $\frac{\pi}{\Omega} \ll < t_{1\to -1} > (\tau = 0)$, then the well will change shape and the system will almost surely exit the well at $\tau = \frac{\pi}{\Omega}$ where the mean escape time $< t_{1\to -1} >$ is minimal: The same reasoning can be applied when the system starts near $y_- \approx -1$ at $\tau = \frac{\pi}{\Omega}$. Thus, for small amplitude, the transitions of the system approximately occur when τ is a multiple of $\frac{\pi}{\Omega}$, and the system stochastically resonates with the forcing of angular frequency Ω.

It is unclear whether the Dansgaard-Oeschger events are in fact generated by such a mechanism (the addition of a ∼1500 year periodicity in freshwater forcing is *ad hoc* – we know of no such forcing in reality), but it nonetheless constitutes a fascinating result that ordered behaviour may come out of the addition of white noise.